Korean J. Chem. Eng., 38(1), 121-128 (2021)
DOI: 10.1007/s11814-020-0636-9

pISSN: 0256-1115
eISSN: 1975-7220

Effect of Cu-MOFs incorporation on gas separation of Pebax thin film nanocomposite (TFN) membrane

Mahdi Fakoori*, Amin Azdarpour*,†, Reza Abedini, and Bizhan Honarvar***

*Department of Chemical Engineering, Marvdasht Branch, Islamic Azad University, Marvdasht, Iran
**Faculty of Chemical Engineering, Babol Noshirvani University of Technology, Babol, Iran
(*Received 19 April 2020 • Revised 28 June 2020 • Accepted 11 July 2020*)

Abstract–MOF-based membranes, which have appropriate MOF dispersion and suitable interaction, have shown high CO_2 permeability and significant CO_2/CH_4 and CO_2/N_2 selectivity. In this study, a layer of Pebax was coated on polysulfone (PSF), which this layer incorporated by various content of Cu-MOFs to improve the performance (permeability and CO_2/CH_4 and CO_2/N_2 selectivity) of all membranes. Characterization techniques such as SEM, TGA, BET, and gas adsorption verified that Cu-BTC was successfully dispersed into the Pebax matrix. Pure CO_2 and CH_4 gases permeation experiments were performed to investigate the impact of Cu-MOFs on the gas permeability of prepared MOF-based membranes. The "Pebax" embedded by 15 wt% CuBTC and 15 wt% of NH_2-CuBTC over PSF support exhibited higher gas separation performance compared to the pristine one. They demonstrated a CO_2 permeability of 228.6 and 258.3 Barrer, respectively, while the blank membrane had a CO_2 permeability of 110.6 Barrer. Embedding the NH_2-Cu-BTC intensified the interaction between incorporated MOF particles and the polymer phase that led to increase the CO_2/CH_4 and CO_2/N_2 selectivity. In addition, the performance of prepared membranes was evaluated at various feed pressures with the range of 2-10 bar. The CO_2/CH_4 and CO_2/N_2 separation was enhanced as the feed pressure surged.

Keywords: Cu-MOFs, MOF-based Membrane, Gas Separation Performance

INTRODUCTION

One of the most important concerns of environmental issues is global warming strongly attributed to high carbon dioxide (CO_2) emission caused by manufacturing and fossil-fuel combustion [1,2]. Carbon capture and storage (CCS) is suggested as an efficient solution to reduce CO_2 emission. Besides, CO_2 has been considered as the acidic gas in natural gas stream that has had great effects on pipeline transmission and releasing energy from natural gas. Hence, removing CO_2 from natural gas stream leads to diminishing the corrosion problems in transportation equipment and also increases the heating value of final natural gas sweating [3].

In recent years, common technologies for CCS and CO_2 separation have been developed such as solid adsorption [4], solvent absorption [5], cryogenic separation [6], and membrane-based separation [7,8]. Gas separation membranes have been recognized the most promising owing to being environmentally friendly, energy efficient, flexible operation, and cost effectiveness [9]. Polymeric membranes are currently well-commercialized due to their ease in scale-up and good processability [10-13]. However, the performance of traditional polymeric membranes is limited by a trade-off relationship between selectivity (S) and permeability (P); it means that highly permeable polymeric membranes have low selectivity and vice versa [14,15]. Over the last decades, many studies have been applied for achieving an ideal membrane (i.e., highly selective and very permeable toward specific gas) to overcome this undesirable relationship by using microporous inorganic materials such as covalent organic frameworks (COFs) [16], metal-organic frameworks (MOFs) [17,18], zeolites [19,20], and silica [21,22] in polymeric matrix to improve both selectivity and permeability.

MOFs are a fascinating kind of inorganic porous materials that are synthesized by association of organic linker and metal clusters to make a framework structure. Multifunctionality, extraordinary high thermal stability, low density, high surface area, and tunable pore size have made them promising candidates in gas separation [23-27]. The combination of the advantages of inorganic fillers and polymeric phase can reduce the formation of a number of defects, including poor dispersion, phase separation, and particle agglomeration [28]. Recently, many studies have been developed in terms of fabrication of thin film nanocomposite (TFN), including a highly permeable porous substrate and a thin selective layer for gas separation applications. High selectivity along with high permeability value is the main feature of TFNs, which makes them superior in comparison with mixed matrix membranes (MMMs). The TFNs comprising Pebax/Zr-MOF over the polymethyl pentene (PMP) support were developed to improve the CO_2/CH_4 separation under various conditions. The CO_2/CH_4 separation was enhanced as the feed pressure increased so that the CO_2 permeability of 393.8 Barrer and CO_2/CH_4 selectivity of 39.8 were achieved for TFN membranes containing 1.5 wt% of Zr-MOF at feed pressure of 7 bar [29]. TFNs incorporated by polymethyl methacrylate (PMMA) grafted multi-walled carbon nanotubes (MWNTs) were used for CO_2/CH_4 and CO_2/N_2 separation. TFN incorporated with PMMA grafted MWNTs presented 29% increment in CO_2 permeance at

†To whom correspondence should be addressed.
E-mail: aminazh22@gmail.com, amin.azhdarpour@miau.ac.ir

70.5 GPU with 9% and 47% enhancement in CO_2/CH_4 and CO_2/N_2 selectivity, respectively, compared to the thin film composite one [30]. The effect of UiO-66-NH_2 decorated by carbon nanofibers (CNFs) on Pebax ®1657 TFN membranes was studied. The resulting TFN membranes exhibited a higher CO_2 permeability as well as appropriate CO_2/CH_4 selectivity compared to TFC membrane. Thus, the TFN membranes demonstrated exceptional separation performance in terms of overcoming the Robeson upper bound [31].

Polyether block amide (Pebax) is a thermoplastic polymer containing polyamide (PA) and poly ethylene oxide (PEO) segments. The high CO_2 affinity and proper filler/polymer compatibility of PEO and high thermal properties of PA hard segments make Pebax the best candidate for formation of selective layer over the substrate [29]. $Cu_3(BTC)_2$ (also known as HKUST-1) is one of the well-known MOFs which is comprised of Cu^{2+} cluster coordinated by carboxylate groups of 1,3,5-benzentricarboxylate acid as a ligand to form a paddlewheel type metal corners bounded to four tricarboxylate linkers. The crystalline structure of $Cu_3(BTC)_2$ has large central cavities (pore size of 9 Å) surrounded by small pockets (pore size of 5 Å). These side channels are connected through triangular windows of 3.5 Å, which forms the central cage of crystal structure [18]. The metal core fulfills its lack of electrons through a weak bond and its axial coordination site is occupied by lone pair solvent molecule. Consequently, these building blocks form a three-dimensional cubic framework with open pore system through BTC ligands. Ease of synthesis and chemical stability are considered as the main features of this MOF. Meanwhile, good affinity to CO_2 molecules due to unsaturated metal sites that would be available after the activation step is another characteristic of $Cu_3(BTC)_2$ [32].

Additionally, Cu-BTC (copper (II) benzene-1,3,5-tricarboxylate) is used in polymer matrix as the potential MOF candidate for CO_2 separation. Cu-BTC frameworks, a face centered-cubic crystals with three dimensional microporous network, are synthesized by coordination of benzene-1,3,5-tricarboxylate ligands and copper cations [30].

In the present work, we proposed to improve gas separation performance of a neat thin-film membrane of PSF/Pebax (PSF and Pebax act as substrate and thin selective layer, respectively) by embedding Cu-BTC particles. To enhance further CO_2 adsorption of Cu-BTC, amine modification of ligand was investigated. The main objective of current study was to obtain a suitable combination of high selectivity and high permeability. Gas permeation parameters under various feed pressure were evaluated in detail. Furthermore, the prepared membranes were characterized utilizing diverse spectroscopic, microscopic, diffraction, and gravimetric approaches as a good exhibition of filler/polymer coalition.

MATERIALS AND METHODS

1. Materials

Polysulfone (PSF) was supplied from Solvay and was used for substrate preparation. Pebax was purchased from Arkema (France). Moreover, 1,3,5-benzenetricarboxylic acid (BTC), 2-aminoterephthalic acid (NH_2-BDC), Copper (II) nitrate trihydrate ($Cu(NO_3)_2 \cdot 3H_2O$), N,N-Dimethylformamide (DMF), 1-Methyl-2-pyrrolidone (NMP), Polyvinylpyrrolidone (PVP), Thiamine pyrophosphate (TPP) and Ethanol were provided from Merck (German).

2. MOFs Synthesis

To synthesize Cu-BTC particles, 1.2 g BTC and 2.4 g $Cu(NO_3)_2 \cdot 3H_2O$ were dissolved in a mixture of 20 mL ethanol, 20 mL DMF, 20 mL bi-distilled water in a beaker. It was followed by 30 min of stirring and heating in a Teflon-lined steel autoclave at 85 °C for 20 h. The gained blue crystals were washed with DMF and first dried at 60 °C for 24 h and then at 120 °C overnight. To synthesize the Cu-BTC with amine functional group (Cu-BTC-NH_2), a similar procedure was conducted with a replacement of 0.3 g NH_2-BDC and 0.9 g BTC mixture instead of 1.2 g BTC as the ligands.

3. Fabrication of Substrate and MOF-based Membranes

The substrate was synthesized by conventional phase inversion. Accordingly, the casting solution was provided by 1% (w/w) PVP, 2% (w/w) TPP, and 14% (w/w) PSF. The casting film was immersed into a water bath for non-solvent/solvent exchange, and the prepared membrane then was kept in water for synthesis of MOF-based membrane, for which to fabricate them; the dope solution was obtained by dispersing Cu-BTC and NH_2-Cu-BTC in ethanol/water at specific concentration and Pebax then added into the solution under reflux condition. The MOF-based membranes were fabricated by soaking PSF substrate into abovementioned dope solution. The composition of each membrane is represented in Table 1.

4. MOFs and Membranes Characterization

Cross section and surface morphology of the membranes were evaluated by means of SEM (MIRA3 TESCAN) at 15 kV. The thermal property of synthesized membranes and fillers was assessed by using TGA (TGA Mettler Toledo) where the membranes were heated from ambient to 600 °C under nitrogen flow. The textural property of MOF was studied by utilization of Belsorp mini II at 77 K. Before experiment, the samples were heated to 90 °C and then the data was recorded in relative pressure range of 0.01 to 1.0 bar. The CO_2 and CH_4 adsorption isotherms study were investigated for fillers and MOF-based membranes, which data were conducted in pressure range of 0-20 bar.

5. Adsorption Test

CO_2, CH_4 and N_2 adsorption isotherms were measured by an automatic apparatus (Tristar II Micromeritics). For each run, 0.5 g of MOF particles was positioned in a sample container at 303 K.

Table 1. Composition details of each blank and MOF-based membranes

Membrane	Polymer phase	
	Pebax (wt%)	MOF (wt%)
PSF/Pebax	100	0
PSF/Pebax_Cu-BTC	99.5	2
PSF/Pebax_Cu-BTC	99	5
PSF/Pebax_Cu-BTC	98.5	10
PSF/Pebax_Cu-BTC	98	15
PSF/Pebax_Cu-BTC-NH_2	99.5	2
PSF/Pebax_Cu-BTC-NH_2	99	5
PSF/Pebax_Cu-BTC-NH_2	98.5	10
PSF/Pebax_Cu-BTC-NH_2	98	15

Previous to each adsorption test, the container was degassed with a nitrogen flow. Furthermore, all samples were regenerated in a vacuum oven at 423 K. The adsorption data was recorded at pressure range of 0-10 bar.

6. Gas Permeation Test

The separation performance characteristic of prepared blank and MOF-based membranes was measured by means of a constant pressure/variable volume system. To perform this assessment, pure CH_4 and CO_2 were passed through the membrane cell with determined feed pressure and then the flow rate of gases on the opposite side of membranes was calculated. This experiment was repeated five times for each membrane and the average value was represented. The amount of permeabilities was measured, which was obtained as below:

$$P = \frac{Q \cdot L}{\Delta p \cdot A} \quad (1)$$

where P is the gas permeability (Barrer), Δp is the pressure difference of gas between two sides of membrane (cmHg), A is the effective membrane area (cm^2), L is the thickness of membrane, and Q is the volumetric flow rate of permeate gas (cm^3/s) under standard condition. CO_2/CH_4 ideal selectivity was measured using the following equation:

$$\alpha = \frac{P_A}{P_B} \quad (2)$$

where, P_A and P_B are the permeability of gases of A and B, respectively.

RESULTS AND DISCUSSION

1. MOFs Characterization

Fig. 1 illustrates the nitrogen adsorption/desorption analysis of the synthesized MOFs. As can be seen, the results confirmed the type I isotherm representing the micropore structure and type IV for Cu-BTC and NH_2-Cu-BTC, respectively, as classified by IUPAC. The physical characteristics of MOFs acquired by BET analysis are listed in Table 2. The textural characteristics in terms of BET surface area, total pore volume and pore diameter of NH_2-Cu-BTC were lower than Cu-BTC. The presence of amine groups within the MOF pores is responsible for this property and its impact on free volume of the micropores ultimately influences on the CO_2 permeability improvement compared to CH_4.

CO_2, CH_4 and N_2 adsorption isotherms of the both types of synthesized MOFs were collected and shown in Fig. 2. Cu-BTC and NH_2-CuBTC particles exhibited the calculated CO_2 adsorption of 3.21 and 4.35 mmol/g at 1 bar, respectively. Also, CO_2 adsorption rate increased upon increasing pressure value. Consequently, as displayed in Fig. 2, Cu-BTC and NH_2-Cu-BTC powders showed the measured CO_2 adsorption value of 16.35 and 15.98 mmol/g at 10 bar, respectively. The results indicated that the CO_2 adsorption uptake of Cu-BTC particles would be more than adsorption uptake of NH_2-Cu-BTC at higher pressure. Furthermore, the maximum CH_4 and N_2 adsorption was attained at 10 bar. As shown in Fig. 2, CO_2 uptake of CuBTC and NH_2-CuBTC increased with raising the adsorption pressure. The strong interaction among positive charges on the unsaturated open Cu and quadro-polarity of CO_2 tends to a significant amount of CO_2 adsorption. CO_2 adsorption isotherm showed that CuBTC has superior potential to adsorb CO_2 than

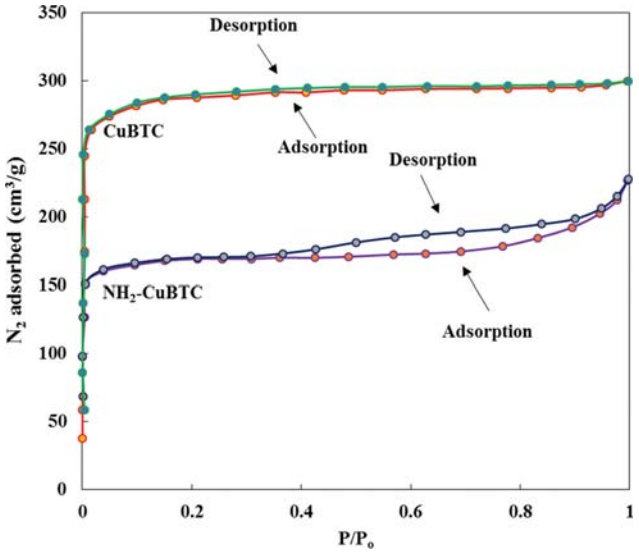

Fig. 1. The nitrogen adsorption/desorption isotherm of MOFs at 77 K.

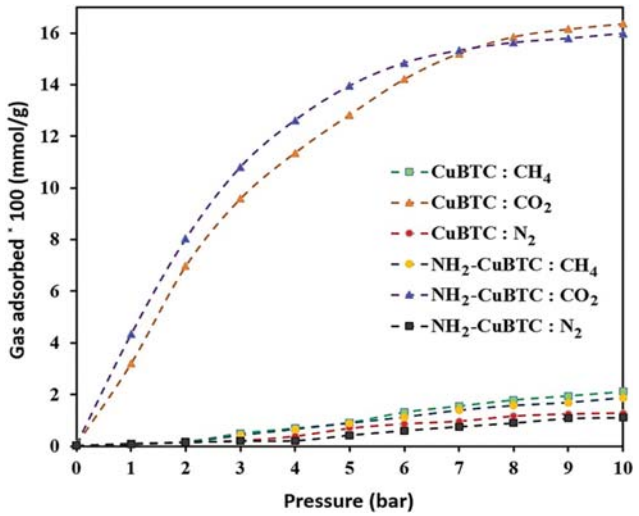

Fig. 2. CO_2, CH_4 and N_2 adsorption isotherms of synthesized Cu-BTC and NH_2-Cu-BTC MOFs.

Table 2. BET analysis of Cu-BTC and NH_2-CuBTC

Sample	S_{BET} (m^2/g)	S_{Micro} (m^2/g)	$V_{Total}{}^a$ (cm^3/g)	V_{Micro} (cm^3/g)	Dp (nm)
Cu-BTC	1,295	964	0.56	0.48	0.89
NH_2-Cu-BTC	672	478	0.33	0.21	0.81

NH_2-CuBTC. This performance affirms the BET data and reported previously for other similar amine-functionalized MOF [30] at pressures lower than 7 bar; higher amount of CO_2 was adsorbed by NH_2-CuBTC compared to CuBTC, mostly owing to presence of -NH_2 group. However, as the feed pressure increased from 7 bar to higher values, the capacity of CO_2 adsorption increased for CuBTC. It could be concluded that at lower pressure the adsorption was controlled by chemical interaction, but at pressure higher than 7 bar, the adsorption mechanism was affected by physical interaction. Therefore, CuBTC with larger pore size can adsorb more CO_2 at higher pressure. For CH_4 and N_2, the amount of CH_4 uptake increased because of increase in adsorption pressure.

2. Characterization of TFN Membranes

TGA study was carried to explore the influence of Cu-MOF fillers on the thermal properties of thin film nanocomposite membranes. Thermograms obtained for Cu-BTC, NH_2-Cu-BTC and fabricated membranes are shown in Fig. 3. As can be seen, the first weight loss region of Cu-BTC occurred in the range of 20-90 °C, which can be attributed to the adsorbed water within the pores. The second region for both Cu-BTC, NH_2-Cu-BTC, which was the weight loss around 310-380 °C, is ascribed to the extra solvent. Furthermore, the TGA diagrams of Pebax 2533 and MOF-based membranes with 10 wt% of Cu-BTC and NH_2-Cu-BTC are presented in Fig. 3. The TGA diagrams of all fabricated membranes include three stages containing the remaining solvent evaporation, the decomposition of polymer chains and eventually the carbonization stage. The thermal decomposition of Pebax 2533 composite membrane begins at 305 °C, but it initiates at lower temperature around 255 °C for TFNs embedded by Cu-MOFs. It is anticipated that the temperature of chain decomposition of fabricated membranes increases as the MOFs content rises owing to the polymer-

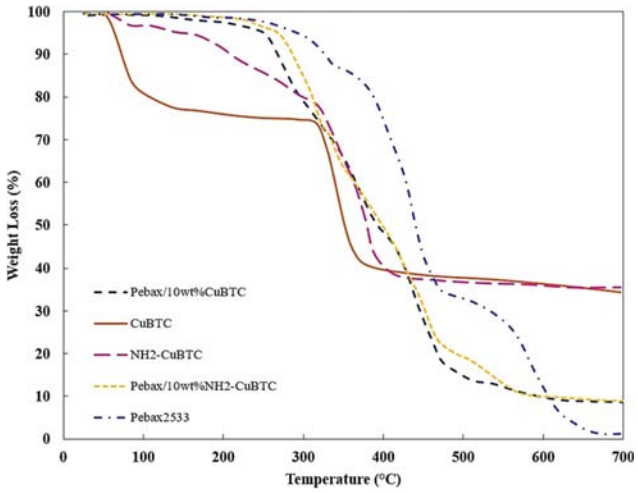

Fig. 3. Thermal gravimetric analysis (TGA) diagram of Cu-BTC, NH_2-Cu-BTC, blank and MOF-based membranes containing 10 wt% of Cu-BTC and NH_2-Cu-BTC.

filler interaction. Nonetheless, the reverse trend takes place for MOF-based membranes and the decomposition temperatures (T_d) drop as the MOFs loading increases. This behavior is ascribed to the difference between the thermal stability of Cu-MOFs and polymer chains. The lower T_d of MOF causes the thermal stability of TFNs become weakened [32,33].

FESEM images were captured to recognize the morphology of membranes, good dispersion of fillers and the properties of polymer/MOF interface. Fig. 4 depicts the surface and cross sectional pictures of MOF-based membrane and cross sectional pictures of Pebax 2533 composite membrane. Based on Fig. 4(f), the Cu-MOF

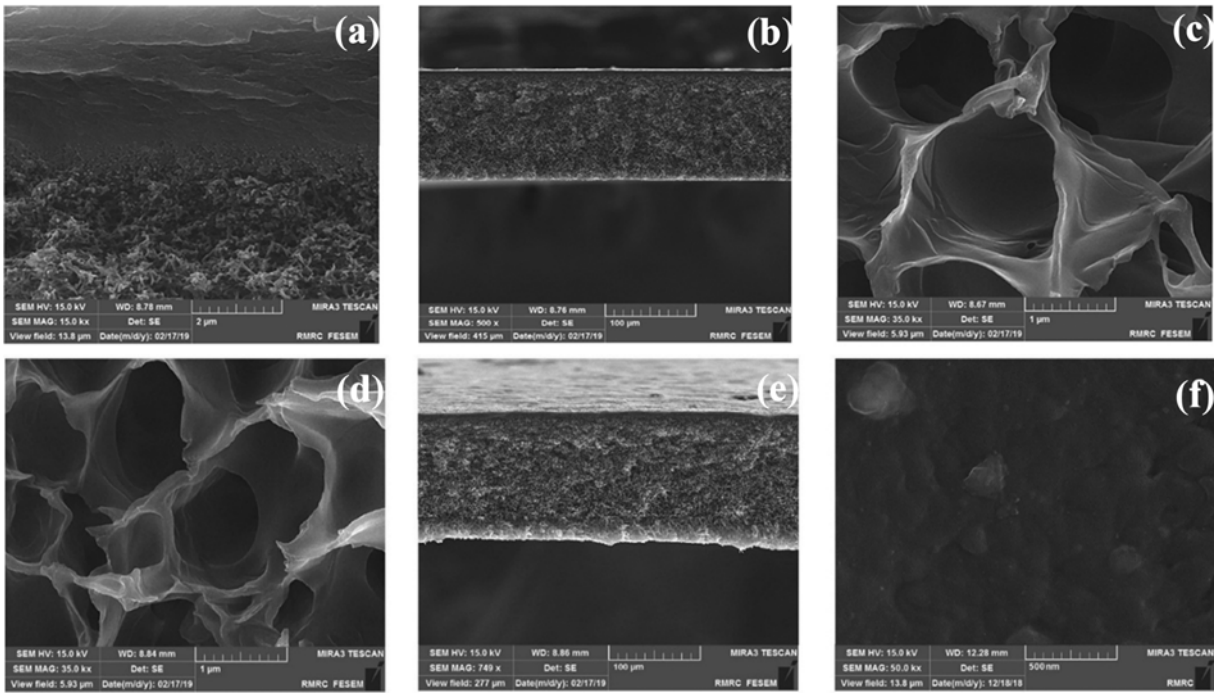

Fig. 4. Surface and cross sectional FE-SEM images of the blank ((a), (b), (c)) and MOF-based membranes ((d), (e), (f)).

nanoparticles are seen clearly as dispersed within the MOF-based membrane surface. However, some particle accumulation can be observed which is possibly due to precipitation of Pebax 2533 on the upper layer of PSF. As presented in Fig. 4(e), the cross sectional morphology of selective thin MOF-based Pebax layer depicts a defect-free feature as well as a uniform structure. Accumulation of MOF particles may cause the creation of non-selective cavities affecting the separation properties of the fabricated TFNs. Consequently, there is no evidence of "sieve-in-a-cage" morphology around the MOFs and so the particles are finely covered by the Pebax chains.

3. Pure Gas Experiments

Pure gas permeation tests of the fabricated blank and MOF-based membranes containing various amounts of Cu-BTC and NH_2-Cu BTC were carried out at 30 °C and feed gas pressure of 6 bar, and the results are presented in Fig. 5. The obtained results show that the CO_2 permeability was considerably higher than CH_4 and N_2 for all fabricated membranes. CO_2 has a lower kinetic diameter and also more condensable than CH_4 and N_2, which tends to the higher permeability [34]. Based on Fig. 5(a), the CH_4 permeability increased upon loading of both Cu-BTC and NH_2-Cu-BTC onto Pebax top layer. According to Fig. 5(c), this trend was repeated for N_2. Although MOF-based membranes containing NH_2-CuBTC particles represented lower CH_4 permeability in comparison with Cu-BTC containing MOF-based membranes, N_2 permeability was similar for both NH_2-Cu-BTC and Cu-BTC containing MOF-based membranes. Lower mean pore size of NH_2-Cu-BTC might be the key factor for greater reduction in CH_4 permeability. As reported in BET results, the amine functionalization of Cu-BTC leads to a pore size reduction, which hinders the larger CH_4 and N_2 to be diffuse. Since CH_4 and N_2 permeate through the membrane via dominant diffusivity, thus NH_2-Cu-BTC incorporation within the membrane results in CO_2 selectivity over CH_4 and N_2. In addition to the lower molecular size of CO_2, the selective CO_2 sorption with Cu-MOFs and the existence of interaction among quadrupole of CO_2 and functional groups of Pebax are the other factors responsible for the higher CO_2 permeability. Fig. 5(a) also reveals that as

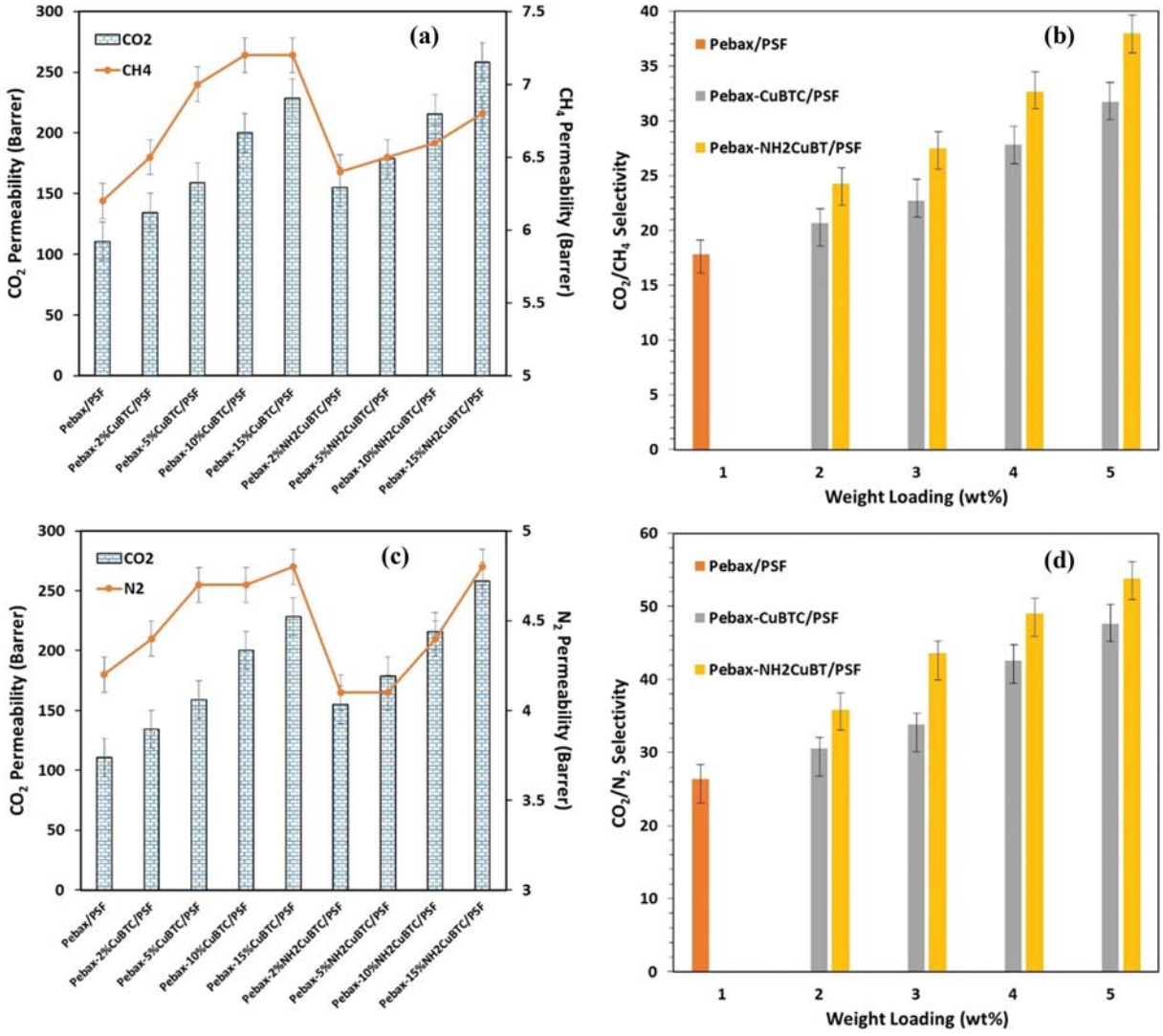

Fig. 5. Pure gas permeability of CO_2 and CH_4 (a), CO_2/CH_4 ideal selectivity (b), Pure gas permeability of CO_2 and N_2 (c), and CO_2/N_2 ideal selectivity (d) of the fabricated blank and MOF-based membranes containing various content of Cu-MOFs at 30 °C and 6 bar.

the MOFs loading increased within the Pebax, the CO_2 permeability was increased due to more interaction among CO_2 and membranes.

Fig. 5(b) and 5(d) show the CO_2/CH_4 and CO_2/N_2 selectivity for fabricated Pebax/PSF and MOF-based membranes. In Fig. 5(b), the blank membrane represents a CO_2/CH_4 ideal selectivity of 17.8, where all MOF-based membranes exhibit higher selectivity upon Cu-MOF incorporation. As the Cu-BTC and NH_2-Cu-BTC content increased to 15 wt%, the CO_2/CH_4 ideal selectivity increased to 31.75 and 38, respectively, at pressure of 6 bar. Also, CO_2/N_2 ideal selectivity for the blank membrane, Pebax-15%-Cu-BTC/PSF and Pebax-15%-NH_2-Cu-BTC/PSF was 26.3, 47.6 and 53.8, respectively. The results listed in Fig. 5(b) prove that the MOF-based membranes incorporated by amine modified Cu-BTC showed higher CO_2/CH_4 selectivity than those containing only Cu-BTC particles, particularly at the content of 15 wt%. The R-NH_2 group of NH_2-Cu-BTC MOFs can interact with polar CO_2 reversibly to form carbonate group. Thus, the CO_2 permeability would increase and as a result the CO_2/CH_4 selectivity improves. Moreover, the -NH_2 groups would improve the adaptability between Pebax chain and MOFs, which would strengthen the chain stiffening surrounding the MOFs. This superior compatibility between MOFs particles and Pebax chain due to the -NH_2 group was reported previously by Mozafari et al. [29]. Moreover, the effect of -NH_2 groups on the strengthened and the better interface quality of NH_2-MIL 53/polyimide and NH_2-MIL53/PMP was described by Chen et al. [30].

The effect of feed pressure on gas permeability, CO_2/CH_4 and CO_2/N_2 selectivity was studied for all fabricated membranes and the obtained data are shown in Fig. 6. For all TFNs except Pebax-15%NH_2-Cu-BTC/PSF, the CO_2 permeability increased by increasing the feed pressure, while the CH_4 and N_2 permeability remained constant during experiments, which confirmed their independency of feed pressure. As can be clearly seen in Fig. 6, the CO_2 permeability for Pebax-15%Cu-BTC/PSF and Pebax-15%NH_2-Cu-BTC/PSF increased from 214.6 and 232.7 Barrer to 255.8 and 253.4 Barrer, respectively, while the feed gas pressure increased from 2 to 10 bar. In fact, the concentration of condensable CO_2 in the polymer increased at higher feed gas pressure and the permeability was enhanced due to plasticization effect. Furthermore, the CO_2

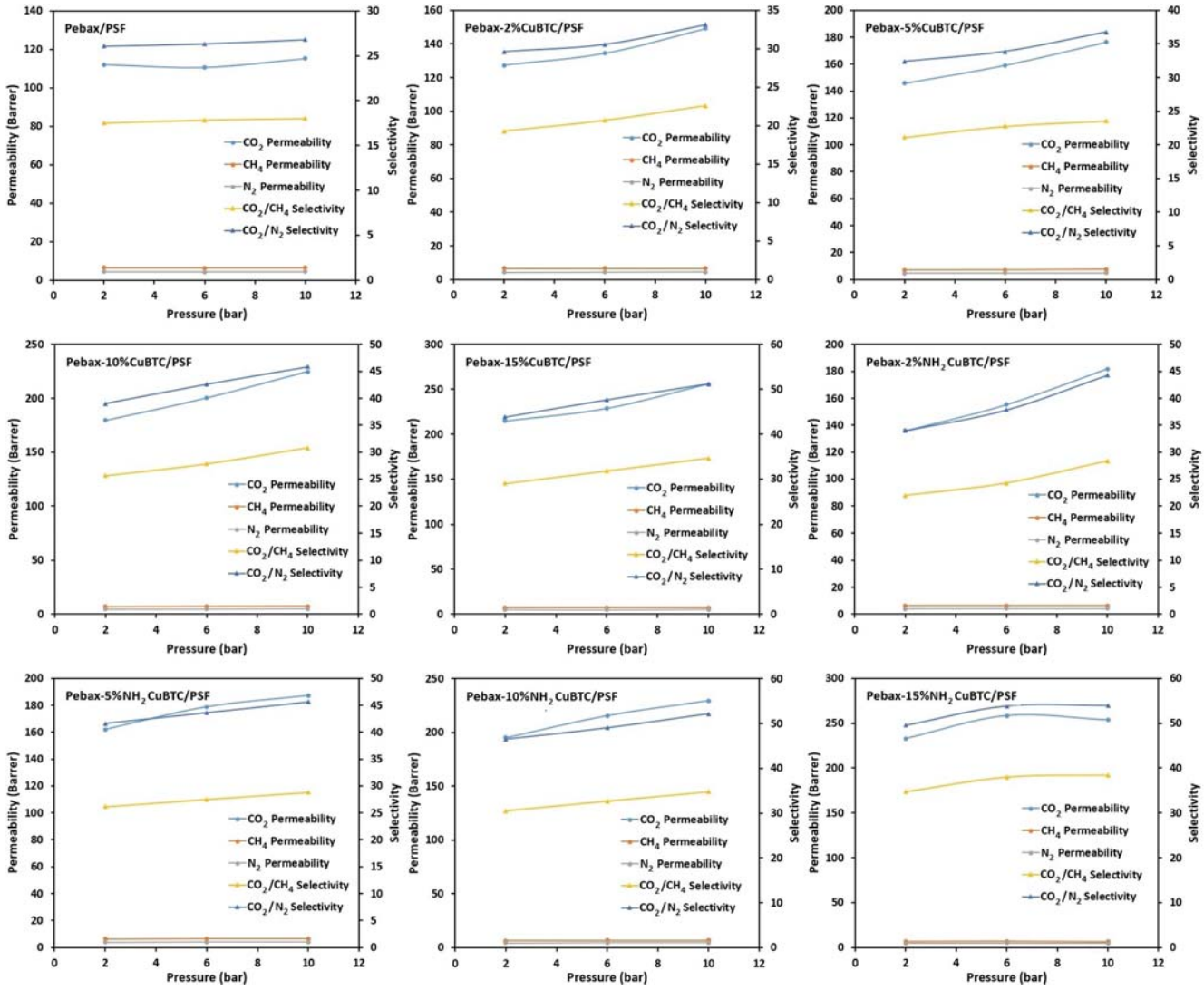

Fig. 6. The influence of pressure on gas permeability and selectivity of fabricated TFN membranes.

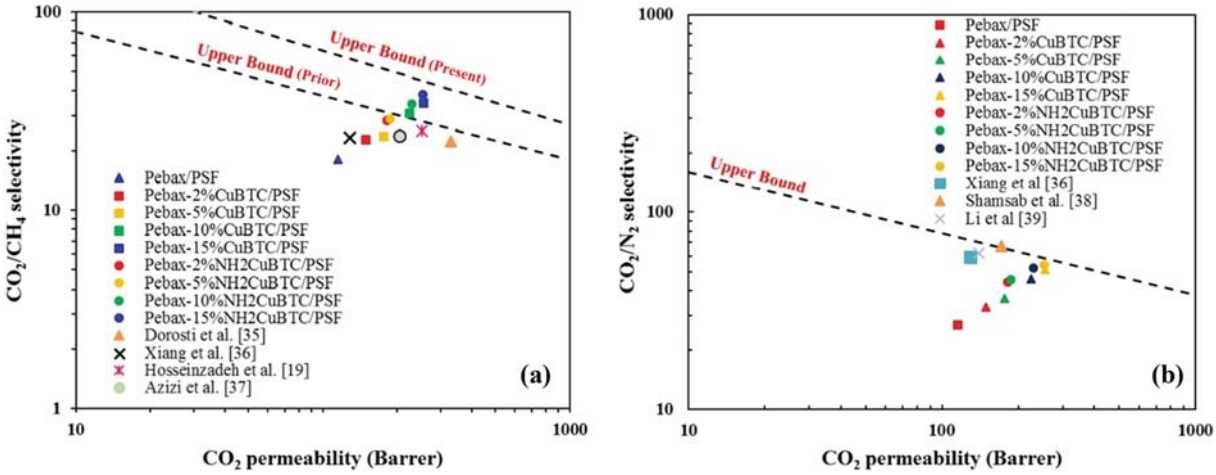

Fig. 7. Comparison of performance of blank and MOF-based membranes with Robeson upper bound based on (a) CO_2/CH_4 and (b) CO_2/N_2 selectivity.

sorption onto MOF surface increased upon increasing feed pressure which caused the CO_2 permeability to improve.

Based on the dual sorption theory, the gas diffusion declines before CO_2-induced plasticization takes place, owing to the polymer chain compactness. Thus, the CO_2 molecules go through the membrane wall by embedding sorption and condensation mechanisms. As a matter of fact, below the plasticization pressure, there is a rivalry between Cu-MOF particles and Pebax-based membrane matrix for CO_2 sorption.

Fig. 7(a) and 7(b) demonstrate the performance of fabricated blank and MOF-based membranes in CO_2/CH_4 and CO_2/N_2 separation at pressure of 6 bar with respect to the Robeson bound. The bounds in Figs. 7(a) and 7(b) demonstrate the existence of a trade-off relation between selectivity and permeability, which improvement in one of them is subjected to the decline of the other. As can be understood, the CO_2/N_2 performance of membranes comprised of 10 and 15 wt% of Cu-MOFs clearly approached the bound. The general trend of CO_2 permeability versus CO_2/CH_4 and CO_2/N_2 selectivity represents the behavior against the Robeson bound trade-off.

CONCLUSIONS

High CO_2/CH_4 separation performance was represented by novel MOF-based membranes, including PSF as substrate, incorporating Pebax matrix as selective layer and Cu-MOFs as particles. This approach caused a surge in both permeability and selectivity because of appropriate interfacial interaction between polymer chains and Cu-MOFs and high CO_2 adsorption. It obviously could be concluded that CO_2/CH_4 selectivity and permeability were enhanced by embedding Cu-MOFs and applying high feed pressure simultaneously. Furthermore, better separation performance was indicated by utilization of amine modified Cu-BTC in comparison to Cu-BTC and blank membrane.

ACKNOWLEDGEMENT

The authors gratefully acknowledge the financial support of Islamic Azad University, Marvdasht, Iran.

REFERENCES

1. S. Choi, J. H. Drese and C. W. Jones, *ChemSusChem: Chem. Sustainability Energy Mater.*, **2**, 796 (2009).
2. K. Shahrezaei, R. Abedini, M. Lashkarbolooki and A. Rahimpour, *Korean J. Chem. Eng.*, **36**, 2085 (2019).
3. U. W. Siagian, A. Raksajati, N. F. Himma, K. Khoiruddin and I. G. Wenten, *J. Nat. Gas Sci. Eng.*, **67**, 172 (2019).
4. L. A. Pellegrini, G. De Guido and V. Valentina, *J. Nat. Gas Sci. Eng.*, **61**, 303 (2019).
5. O. Aschenbrenner and P. Styring, *Energy Environ. Sci.*, **3**, 1106 (2010).
6. M. Tuinier, M. van Sint Annaland, G. J. Kramer and J. Kuipers, *Chem. Eng. Sci.*, **65**, 114 (2010).
7. J. Lee, J. Kim, H. Kim, K. S. Lee and W. Won, *J. Nat. Gas Sci. Eng.*, **61**, 206 (2019).
8. M. H. Nematollahi, S. Babaei and R. Abedini, *Korean J. Chem. Eng.*, **36**, 763 (2019).
9. P. Bernardo, E. Drioli and G. Golemme, *Ind. Eng. Chem. Res.*, **48**, 4638 (2009).
10. J. Dechnik, J. Gascon, C. J. Doonan, C. Janiak and C. J. Sumby, *Angew. Chem. Int. Ed.*, **56**, 9292 (2017).
11. D. Bastani, N. Esmaeili and M. Asadollahi, *J. Ind. Eng. Chem.*, **19**, 375 (2013).
12. H. B. T. Jeazet, C. Staudt and C. Janiak, *Dalton Trans.*, **41**, 14003 (2012).
13. S. Wang, X. Li, H. Wu, Z. Tian, Q. Xin, G. He, D. Peng, S. Chen, Y. Yin and Z. Jiang, *Energy Environ. Sci.*, **9**, 1863 (2016).
14. L. M. Robeson, *J. Membr. Sci.*, **320**, 390 (2008).
15. B. D. Freeman, *Macromolecules*, **32**, 375 (1999).
16. R. Babarao and J. Jiang, *Energy Environ. Sci.*, **1**, 139 (2008).
17. R. Abedini, A. Mosayebi and M. Mokhtari, *Process Saf. Environ. Prot.*, **114**, 229 (2018).
18. K. Pirzadeh, A. A. Ghoreyshi, M. Rahimnejad and M. Mohammadi, *Korean J. Chem. Eng.*, **35**, 974 (2018).

19. H. Hosseinzadeh Beiragh, M. Omidkhah, R. Abedini, T. Khosravi and S. Pakseresht, *Asia-Pacific J. Chem. Eng.*, **11**, 522 (2016).
20. T. W. Pechar, S. Kim, B. Vaughan, E. Marand, M. Tsapatsis, H. K. Jeong and C. J. Cornelius, *J. Membr. Sci.*, **277**, 195 (2006).
21. E. Nezhadmoghadam, M. Pourafshari Chenar, M. Omidkhah, A. Nezhadmoghadam and R. Abedini, *Korean J. Chem. Eng.*, **35**, 526 (2018).
22. T.-H. Weng, H.-H. Tseng and M.-Y. Wey, *Int. J. Hydrogen Energy*, **35**, 6971 (2010).
23. X. Zou, H. Ren and G. Zhu, *Chem. Commun.*, **49**, 3925 (2013).
24. X. Zou and G. Zhu, *Adv. Mater.*, **30**, 1700750 (2018).
25. X. Feng, X. Ding and D. Jiang, *Chem. Soc. Rev.*, **41**, 6010 (2012).
26. S.-Y. Ding and W. Wang, *Chem. Soc. Rev.*, **42**, 548 (2013).
27. A. I. Cooper, *Adv. Mater.*, **21**, 1291 (2009).
28. R. Mahajan and W. J. Koros, *Ind. Eng. Chem. Res.*, **39**, 2692 (2000).
29. M. Mozafari, R. Abedini and A. Rahimpour, *J. Mater. Chem. A*, **6**, 12380 (2018).
30. K. C. Wong, P. S. Goh and A. F. Ismail, *Int. Biodeterior. Biodegrad.*, **102**, 339 (2015).
31. M. Mozafari, A. Rahimpour and R. Abedini, *J. Ind. Eng. Chem.*, **85**, 102 (2020).
32. K. Pirzadeh, K. Esfandiari, A. A. Ghoreyshi and M. Rahimnejad, *Korean J. Chem. Eng.*, **37**, 513 (2020).
33. S. R. Venna, M. Lartey, T. Li, A. Spore, S. Kumar, H. B. Nulwala, D. R. Luebke, N. L. Rosi and E. Albenze, *J. Mater. Chem. A*, **3**, 5014 (2015).
34. Q. Yang, A. D. Wiersum, P. L. Llewellyn, V. Guillerm, C. Serre and G. Maurin, *Chem. Commun.*, **47**, 9603 (2011).
35. F. Dorosti and A. Alizadehdakhel, *Chem. Eng. Res. Des.*, **136**, 119 (2018).
36. L. Xiang, Y. Pan, G. Zeng, J. Jiang, J. Chen and C. Wang, *J. Membr. Sci.*, **500**, 66 (2016).
37. N. Azizi, M. R. Hojjati and M. M. Zarei, *Silicon*, **10**, 1461 (2018).
38. A. Arabi Shamsabadi, F. Seidi, E. Salehi, M. Nozari, A. Rahimpour and M. Soroush, *J. Mater. Chem. A*, **5**, 4011 (2017).
39. X. Li, Z. Jiang, Y. Wu, H. Zhang, Y. Cheng, R. Guo and H. Wu, *J. Membr. Sci.*, **495**, 72 (2015).